life

MDPI

Article

RETRACTED: Metal Catalysis Acting on Nitriles in Early Earth Hydrothermal Systems

Miranda Sturtz * and Christopher House *

Department of Geosciences, Pennsylvania State University, 116 Deike Building, University Park, PA 16802, USA
* Correspondence: mbs6874@psu.edu (M.S.); chh10@psu.edu (C.H.)

Abstract: Hydrothermal systems are areas in which heated fluids and organic molecules rush through basaltic material rich in metals and minerals. By studying malononitrile and acetonitrile, we examine the effects of metal and mineral nanoparticles on nitrile compounds in anoxic, hydrothermal conditions representing a prebiotic environment of early Earth. Polymerization, reduction, cyclization, and a phenomenon colloquially known as 'chemical gardening' (structure building via reprecipitation of metal compounds or complexing with organics) are all potential outcomes with the addition of metals and minerals. Reduction occurs with the addition of rhodium (Rh) or iron (II) sulfide (FeS), with positive identification of ethanol and ethylamine forming from acetonitrile reduction. We find that polymerization and insoluble product formation were associated with oxide minerals, metallic nickel (Ni), and metallic cobalt (Co) acting as catalysts. Oxide minerals strongly promoted polymerization into insoluble, tar-like products of nitriles. FeS, iron-nickel alloy (FeNi), and rhodium are unique cases that appear to act as reagents by actively participating in chemical gardening without returning to their initial state. Further, FeS tentatively had a phase change into the mineral parabutlerite. This research aims to identify metals and metal minerals that could best serve nitrile catalysis and reactions on early Earth.

Keywords: metal catalysis; nitriles; hydrothermal systems; minerals; polymerization; prebiotic chemistry; chemical gardening

Citation: Sturtz, M.; House, C. RETRACTED: Metal Catalysis Acting on Nitriles in Early Earth Hydrothermal Systems. *Life* **2023**, *13*, 1524. https://doi.org/10.3390/life13071524

Academic Editors: Ranajay Saha and Alberto Vázquez-Salazar

Received: 5 June 2023
Revised: 27 June 2023
Accepted: 5 July 2023
Published: 7 July 2023
Retracted: 26 March 2024

1. Introduction

While the exact environment of an early Earth is difficult to predict, global oceans were thought to have areas of hydrothermal systems in which heated water flowed through basaltic rock. These off-axis, oceanic hydrothermal systems have garnered much attention as potential environments where life may have originated. The hypothesis of origin of life processes in undersea vents is due to processes such as serpentinization and organic molecules mixing with basaltic minerals from crustal processes [1–5]. These systems could have provided an aqueous environment where organic molecules could combine with heat to produce products such as amino acids and nucleotides [6,7]; ketones, aldehydes, and sugars [7]; hydrogen cyanide (HCN) polymers [8,9]; and reduced nitrogen species [10]. A common pool of organic compounds may have been available to form early genetic molecules and metabolism cycles. Hydrothermal systems provide a direct channel in which heated water circulates while in contact with basaltic rock [3]. Of the metals in basaltic systems, the most notable and accessible by potential prebiotic reactions are the transition metals, either as metallic constituents or as oxides and sulfide minerals [4,11–14]. In an early Earth ocean, these metals may have been found in their native states within serpentinites forming at hydrothermal systems active in serpentinization [2].

Hydrogen cyanide (HCN) is thought to have been prevalent in the early Earth atmosphere from the photochemical interaction between molecular nitrogen (N_2) and methane (CH_4). HCN production in the upper atmosphere would have resulted in the rainout

This paper has been retracted. A retraction notice was published on 26 March 2024 in *Life* **2024**, *14*, 439. https://doi.org/10.3390/life14040439

of HCN, with production rates of up to 1×10^7 cm^{-2} s^{-1} or 30 Tg/yr. [15]. If concentrated, HCN can yield polymerization and degradation into formic acid and further into hydrogen and carbon dioxide. Polymerization of HCN leads to a dimer (iminoacetonitrile, $C_2H_2N_2$), trimer (aminomalononitrile, $C_3H_3N_3$), and tetramer (diaminomaleonitrile, DAMN, $C_4H_4N_4$) (Figure 1) [8]. Another potential fate of HCN is the formation of amino acids via the Strecker synthesis pathway [16,17]. Overall, the nitrile family is an attractive group of molecules to study due to their relative abundance in the early Earth oceans, high reactivity, presence in meteorites [8], and relevance to prebiotic molecules.

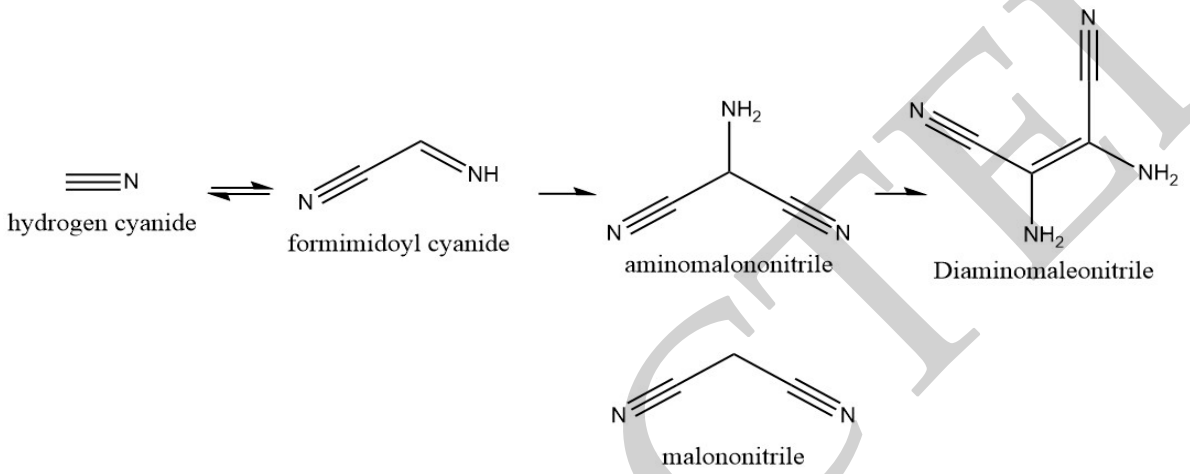

Figure 1. Self-polymerization of hydrogen cyanide (HCN). Under hydrothermal conditions and high concentrations, HCN polymerization of the monomer into the dimer (iminoacetonitrile) is spontaneous and reversible. Polymerization to the trimer (aminomalononitrile) and further into the tetramer (DAMN) is also spontaneous but is not a reversible reaction. Note the comparison of aminomalononitrile (**above**) to malononitrile (**below**) and the lack of an amine group on the second carbon of malononitrile.

This study uses the dinitrile malononitrile as a simpler analog molecule to the prebiotically relevant trimer, aminomalononitrile. It would be ideal to study aminomalononitrile itself; however, the additional amine group makes the compound highly reactive and unstable. For example, aminomalononitrile is prone to self-polymerization under otherwise stable conditions [18]. Malononitrile ($C_3H_2N_2$) is a three-carbon molecule with two terminal nitrile groups that resembles aminomalononitrile without the amine group (Figure 1). Malononitrile was chosen as a model molecule to study the dinitrile group reactions while avoiding additional polymerization from other functional groups. Malononitrile is the simplest dinitrile that could be used in this experimentation for examination of hydrolysis, polymerization, and alternative reaction pathways via metal and mineral additions. The smaller two-carbon dinitrile cyanogen is a highly toxic gas that did not suit the experimental layout of this study.

The metals and minerals used in the experimental setup of this study (Table 1) were chosen primarily for their geologic relevance or catalytic capabilities in previous studies. This study pursued lesser examined metals and metal minerals. Previous prebiotic studies have utilized reduced ferrous iron (Fe^{2+}) as a metallic catalyst due to the predicted high concentrations in the oceanic water column and crust during the Archean [19], as well as due to its relevance to virtually all known extant biology [20]. An iron–nickel alloy (FeNi) provided use of metallic nickel and metallic iron, which are found in serpentinites. While rare on Earth, FeNi is found to commonly occur in asteroids and meteorites. This alloy represents a potential metal source delivered to the oceans via meteor impacts [21]. Iron (II) sulfide (FeS) provides Fe^{2+} in mineral form. Out of all the metals and minerals presented, FeS is considered the most geologically relevant mineral for hydrothermal systems on the early Earth of the additions presented [11]. Cobalt (Co) and nickel (Ni) were

chosen to represent first row transition metals in early Earth basaltic material at off-axis points [12,22]. In order to compare metallic activity trends on nitriles from similar periodic groups, rhodium (Rh) was used to compare with the cobalt organic products [23].

Other minerals include the oxides titanium oxide (TiO_2) and aluminum oxide (α-Al_2O_3). Although it is unknown what quantities of TiO_2 or Al_2O_3 an anoxic early Earth basaltic system would have had, these oxides are common in modern oxic oceans and sediments. Titanium is the fourth most abundant element in Earth's crust today; TiO_2 (rutile) is a naturally occurring mineral and is one of the most common mineral forms of titanium [24]. α-Al_2O_3 is another of the most common oxides in the modern day Earth's crust and in hydrothermal systems [25]. Thus, these metal oxides were included within the study to be able to characterize the effects of an oxidized mineral on the nitrile compounds under the same conditions as the more relevant minerals and elemental metals.

Table 1. Characteristics of metals and minerals used.

Catalyst	Size	Notes	Common Uses	References
Aluminum oxide (Al_2O_3)	≤10 µm nanopowder	Primarily α-phase (trigonal crystal structure) [+]	Highly determinate on surface area; dehydration of alcohols to alkenes; may allow for organic adsorption onto mineral surfaces	[25,26]
Cobalt (Co)	≤15 µm nanopowder	N/A	Rarely used in elemental form; carbonyl complex in Fischer–Tropsch synthesis	[27]
Iron (II) sulfide (FeS)	Technical grade powder (ground into ≤15 µm nanopowder)	Primarily as troilite (hexagonal crystal structure) [++]	Participates with O_2 and H_2S in oxidation cycles; degrades organics via the iron sulfide Fenton process (with H_2O_2); electrochemical H evolution	[28–33]
Iron–nickel Alloy (FeNi)	≤10 µm nanopowder	N/A	Hydrogen generation and ammonia synthesis at high temperatures	[34,35]
Nickel (Ni)	≤10 µm nanopowder	N/A	Wide range of reductions including aldehyde/ketone and nitrile reductions; hydrolysis; alkene hydrogenation	[36–43]
Rhodium (Rh)	Technical grade powder (ground into ≤15 µm nanopowder)	Matrix alumina support; 5% Rh by weight [+]	Selective C-C double bond hydrogenation when in hydride form; N_2O decomposition	[44,45]
Titanium (IV) oxide (TiO_2)	≤10 µm nanopowder	Primarily as rutile (tetragonal crystal structure) [+]	Chemically inert; may be reduced to metallic state via heating and hydrogen flow; may allow for organic adsorption onto mineral surface	[24,25]

[+] As confirmed by manufacturer [++] As confirmed by XRD in this study.

2. Materials and Methods

Reactions were prepared in standard 7.4 pH water degassed from oxygen by bubbling with N_2 gas for 20 min in 500 mL aliquots. The vials were 10 mL borosilicate glass vials with a bottom radius of 1 cm. Incubation was for 48 h either in a 90 °C incubator or at room temperature (20 °C); 90 °C was chosen to reflect mild hydrothermal conditions that would not have been paired with extreme pressures, such as at a serpentinization hydrothermal vent. This temperature also approximated what reactions would have occurred at lower temperatures on too long of a timescale to observe in the laboratory. New 20 mm airtight rubber stoppers (Chemglass Life Sciences) with aluminum seals were used to cap each glass vial to prevent the introduction of oxygen and hydrogen gas leakage. Trace levels of

chemicals could potentially leech from the stoppers into the reaction solution. However, this potential source of organics is minimal compared to concentration of experimental reagents (nitriles, sodium formate, and metals/minerals) used.

All reagents used in this experiment are commercially available. Metals and minerals were all purchased from Sigma-Aldrich in powder form. Metals and minerals were all <150 μm in diameter and categorized as nanoparticles except for rhodium and FeS (Table 1). The FeS chunks were large enough that grinding with a mortar and pestle was required to reach the desired <150 μm particle size. TiO_2 was purchased in the rutile phase, and Al_2O_3 was purchased in the alpha phase. The FeNi alloy was purchased with ratios of 55% iron and 45% nickel. Phases and elemental ratios were confirmed by Sigma-Aldrich's commercial analysis. The FeS was primarily in the hexagonal troilite phase, as confirmed by in-house XRD analysis.belowNickel and cobalt are pure elemental forms. Rhodium is a 4.7–5.1% rhodium surface supported by an inner alumina matrix.

Oxygen-sensitive reagents (Ni, Co, FeS, FeNi) were prepared under anoxic conditions (95% N_2 gas, 5% H_2 gas). Non oxygen-sensitive reagents (Rh, TiO_2, and Al_2O_3) were prepared under ambient laboratory conditions before being brought into anoxic conditions. Malononitrile concentrations were 1 mN per 5 mL reaction. Acetonitrile concentrations were raised to 2 mN to increase the likelihood of reaction. Sodium formate was added at 2 mN per 5 mL reaction in order to keep an excess of reductant available to replicate an early Earth ocean's reducing conditions. A 100% H_2 headspace provided a weakly reducing atmosphere while avoiding the introduction of new carbon molecules into the system. This was achieved by evacuating all gas out of the prepared vials and flushing with H_2 gas three times for 30 s. Upon the final vacuum, the vials were filled with H_2 gas to 1 atm prior to incubation. The experimental pH range was slightly acidic to slightly basic at pH 6.5–pH 8.5. This pH range caused some products, particularly malonic acid, to have a slightly different chemical shift than what is presented in the standard spectra.

Primary identification analysis of products of nitrile reaction were completed via proton nuclear magnetic resonance (^{1}H-NMR) at 400 mHz with a D_2O solvent. Analysis was carried out at ambient room temperatures (20 °C). Samples were run via ^{1}H-NMR on Nano-400 instrumentation with a 5 mm iProbe cryoprobe with an X-nuclei inner coil and ^{1}H outer coil. Data gathering was carried out using the program TopSpin® 4.0 pl6 running on CentOS® 5.0. Spectral data analysis and interpretation were carried out using MestRe Nova software 5.3.1. All NMR equipment was sourced through the Pennsylvania State University in State College, Pennsylvania, United States.

X-ray diffraction patterns of FeS were collected at 40 kV and 40 mA on a 240 mm radius line source [Co K-α 1-2 (1.789010/1.792900 Å)] diffractometer with a reflection-transmission sample stage fitted with an air sensitive sample holder that utilizes a polycarbonate dome. Data were collected with a step size of 0.008° from 10 to 90° 2-theta. The incident optics consisted of a Bragg–Brentano HD® Co optic fitted with 0.04 rad Soller slits, a 4 mm beam mask, and 1/4° and 1° divergence and anti-scatter slits, respectively. The diffracted optics included an X'Celerator® detector with a 2.1223 active length in scanning line mode fitted with 0.04 rad Soller slits and a fixed anti-scatter slit of the following dimensions: 2.5 mm height and 30 mm width. The distance between the slit and detector was 190 mm. Phase ID was carried out using Jade® software (version 8.7) from Materials Data Inc. (MDI) and the International Centre for Diffraction Data (ICDD) PDF4® database. All equipment for XRD was sourced through the Pennsylvania State University in State College, Pennsylvania, United States. Angles and values during the XRD analysis are found in Table S1.

3. Results and Discussion

3.1. Effect of Metal and Metal Compounds on Malononitrile

The metal and mineral reactions all followed the same general product trend. The main products produced from the hydrothermal incubation of malononitrile were from the hydrolysis of nitrile groups. Previous research has shown that nitriles undergo two-step hydrolysis, with amide formation in the first step in the presence of water, and the second

step resulting in a final carboxylic acid from water and liberating NH_3/NH_4^+ [38]. In this study, malononitrile yielded malonamide, malonate (malonic acid), and most likely malonate monoamide, as confirmed via ^{1}H-NMR (Figures S3 and S5) under all conditions. Figure 2 provides a reference image of malononitrile incubated without any metal or mineral additions. Most of the malononitrile in each condition was hydrolyzed into these products, but a small and appreciable amount of malononitrile underwent reaction with the metal or mineral addition supported by observational changes (Table 2) and chemical analysis. As expanded upon below, reduction, polymerization, and potential cyclization are all feasible reaction routes to avoid decompositional hydrolysis.

Figure 2. Malononitrile incubated for 48 h at 90 °C with sodium formate. The uneven coloring is suspended insoluble polymer. A 0.5 cm scale bar is included for reference.

Table 2. Physical observations of metals and minerals on malononitrile.

Catalyst	Observed Results after 90 °C Incubation
Aluminum oxide (Al_2O_3)	Dark brown–black opaque solution, Al_2O_3 turned from white to gray–brown when in contact with reactants, insoluble precipitate formation
Cobalt (Co)	Orange solution, slight insoluble polymerization
Iron (II) sulfide (FeS)	Yellow solution, no insoluble polymerization
Iron–nickel Alloy (FeNi)	Yellow–brown solution, high levels of insoluble polymerization with algae-like consistency
Nickel (Ni)	Yellow–orange solution, high levels of insoluble long-chain polymerization
Rhodium (Rh)	Dark gold solution, no insoluble polymerization
Titanium (IV) oxide (TiO_2)	Dark brown–black opaque solution, TiO_2 turned from white to gray–brown when in contact with reactants, insoluble precipitate formation

After 48 h of 90 °C anoxic incubation, the reactions with cobalt, rhodium, FeS, and FeNi underwent a phenomenon akin to chemical gardening [46–50]. While chemical gardening traditionally uses an anionic starting solution and silicate compounds, this study demonstrated

that reprecipitation and mineralization is possible without silica and without an additional hydroxide or anion [47]. It also supported the idea that dissolution and subsequent reprecipitation with complexed organics is an outcome possible at oceanic hydrothermal localities. By participating in the reaction as a reagent, the metals and minerals did not function as a catalyst as they could not be recovered in the original form. The nanoparticles grew into acicular mineral growths with concentrated nodules on the fractals (see Figures 3 and 4). These self-built structures were not delicate and only broke under strong agitation during sample collection. The storage conditions of the solutions created unique changes to the group nine transition metals, although product yield was not significantly affected. To counter this, ^{1}H-NMR analysis was completed directly at the end of 48 h.

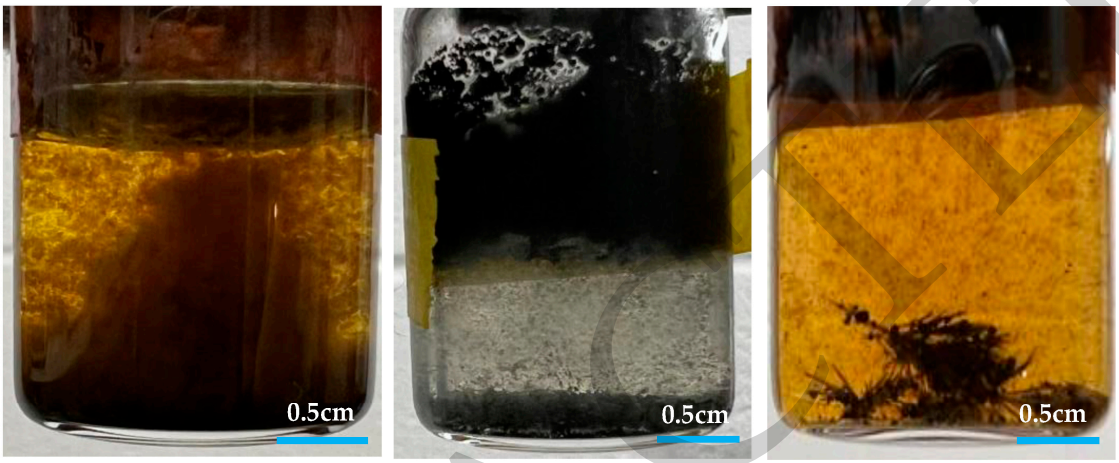

Figure 3. Effects observed with nickel-based reagent addition: (**a**) metallic nickel catalytic effects of algae-like long-chain polymers; (**b**) FeNi alloy effects with no chemical gardening or polymer formation if the alloy remained unmixed; (**c**) FeNi alloy effects with small amounts of polymerization and mineral chemical gardening if the alloy was suspended in the solution via agitation for the duration of the experiment. These reference pictures were taken directly after 48 h at 90 °C. A 0.5 cm scale bar is included for reference.

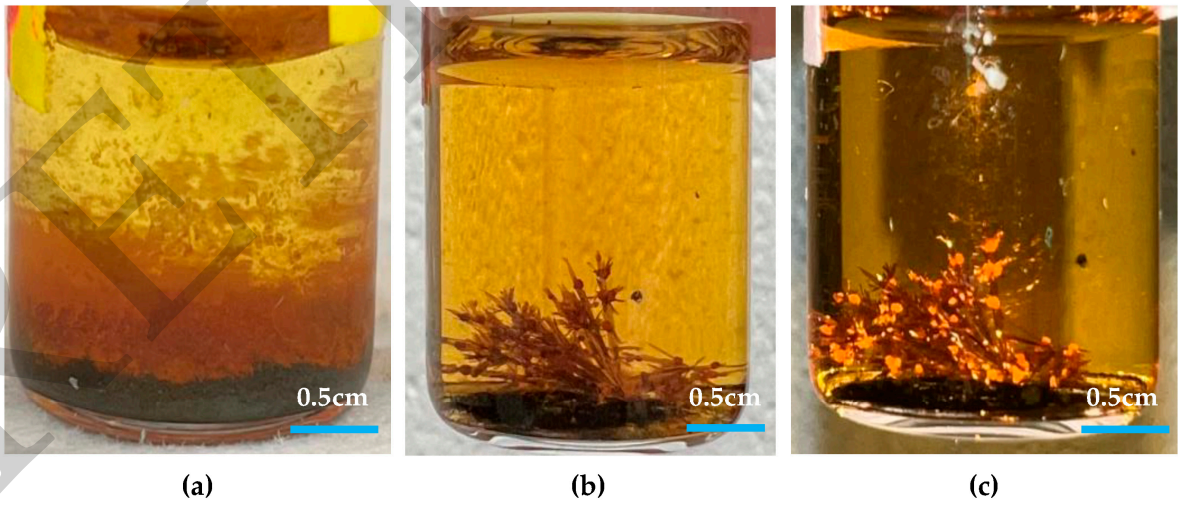

Figure 4. Effects observed with group nine transition metals: (**a**) cobalt catalytic effects with bright orange organic deposition; (**b**) rhodium effects with mineral chemical gardening; (**c**) same sample as in (**b**) with a camera flash to highlight color difference in acicular needles and deposited nodules. These reference pictures were taken directly after 48 h at 90 °C. A 0.5 cm scale bar is included for reference.

3.2. Nickel and FeNi Alloy Addition Observations

Nickel metal can catalyze the reduction of nitrile groups, in addition to formate [36] or metallic iron (Fe) [37], as a reducing agent in aqueous solutions. The addition of hydrogen gas as a reductant with nickel alloys can also reduce nitrile groups into aldehydes and alcohols alike [39–42]. Furthermore, nickel nanoparticles have been shown to catalyze nitrile into aldehydes and alcohols utilizing ammonium formate as the reductant under controlled organic chemistry laboratory conditions [42]. Altogether, these previous studies support the idea that elemental nickel is a strong prebiotic candidate for reduction of the nitrile group into an oxygen-bearing functional group that avoids the formation of carboxylic acids, which decarboxylate over time under hydrothermal conditions.

Nickel nanoparticles became resuspended in the polymers and were unable to settle out without centrifugation (Figure 3a). The nickel nanoparticles acted as a catalyst, enhancing the formation of insoluble polymers from malononitrile, and were not altered. Note that for the FeNi alloy, most of the FeNi alloy nanoparticles remained on the sides of the vial and did not resuspend into the aqueous solution even upon heating (Figure 3b). This may have limited the amount of surface area contact between the alloy particles and the nitrile solution. Full submersion of FeNi was possible from agitation periodically throughout the experiment. While the nickel catalyst did not form any crystal mineral structures, the submerged FeNi alloy particles built acicular mineral growths with terminal nodules via chemical gardening (Figure 3c). This is hypothesized to have been due to the presence of iron in the FeNi alloy, which may have resulted in reprecipitation and remineralization with organic molecules. Our studies concluded that metallic nickel promotes long-chain polymerization of dinitriles into insoluble products and possible reduction of the nitrile group in hydrothermal conditions. FeNi did not promote nor hinder polymerization of malononitrile and had the same amount of visible polymer formation as the control without any metal or mineral addition.

3.3. Cobalt and Rhodium Addition Observations

Rhodium did not produce any visible polymerization suspended in the solution; however, cobalt did produce insoluble orange organics that settled out of solution onto the cobalt nanoparticle layer, pointing towards a catalytic effect that does not appear to change the cobalt itself (Figure 4a). Rhodium chemical gardening had an orange crystalline appearance with bright orange depositions that matched the cobalt precipitants (Figure 4b,c). The nodules on the crystalline acicular growths contrasted with the unreacted black nanoparticles settled at the bottom of the vial. The almost transparent nature of the main acicular mineral growths points towards a hollow state of the acicular needles. Further studies are required for the exact morphology on a nanoscale to determine the differences in opaque nodules and the transparent needles.

While not preventing full polymerization, cobalt promoted a deposition or potential nucleation of polymer to the surface of the nanoparticles (Figure 4a). The addition of rhodium did not result in the formation insoluble products or long chain polymers, and thus the reaction of nitriles must be funneled into an alternative synthesis route, including some reduced products that have not been identified. The lack of insoluble polymer formation in samples with added rhodium was dramatic given that control experiments without any metal or mineral addition showed some polymerization under the conditions used. Ambient room temperature conditions did not produce any mineralization and showed little orange insoluble product production.

3.4. FeS Addition Observations

The iron (II) sulfide, FeS, is the most geologically relevant amongst the tested metals and minerals. Iron sulfide minerals are common in anoxic hydrothermal systems and could have supported an iron–sulfur-based chemical world [33]. For FeS, under hydrothermal conditions (90 °C) for 48 h, there was little polymerization or insoluble product formation. Samples incubated with FeS shifted the nanoparticle appearance from a metallic black

nanopowder to one with metallic orange–gold hues (Figure 5a). Structures formed included creeping orange films that terminated at the upper limit of the catalyst layer and mineral growth from (but not tethered to) the original metallic black catalyst. The organics and FeS most likely underwent chemical gardening or a similar dissolution process, reprecipitating into acicular needles with branching and terminal nodules (Figure 5b).

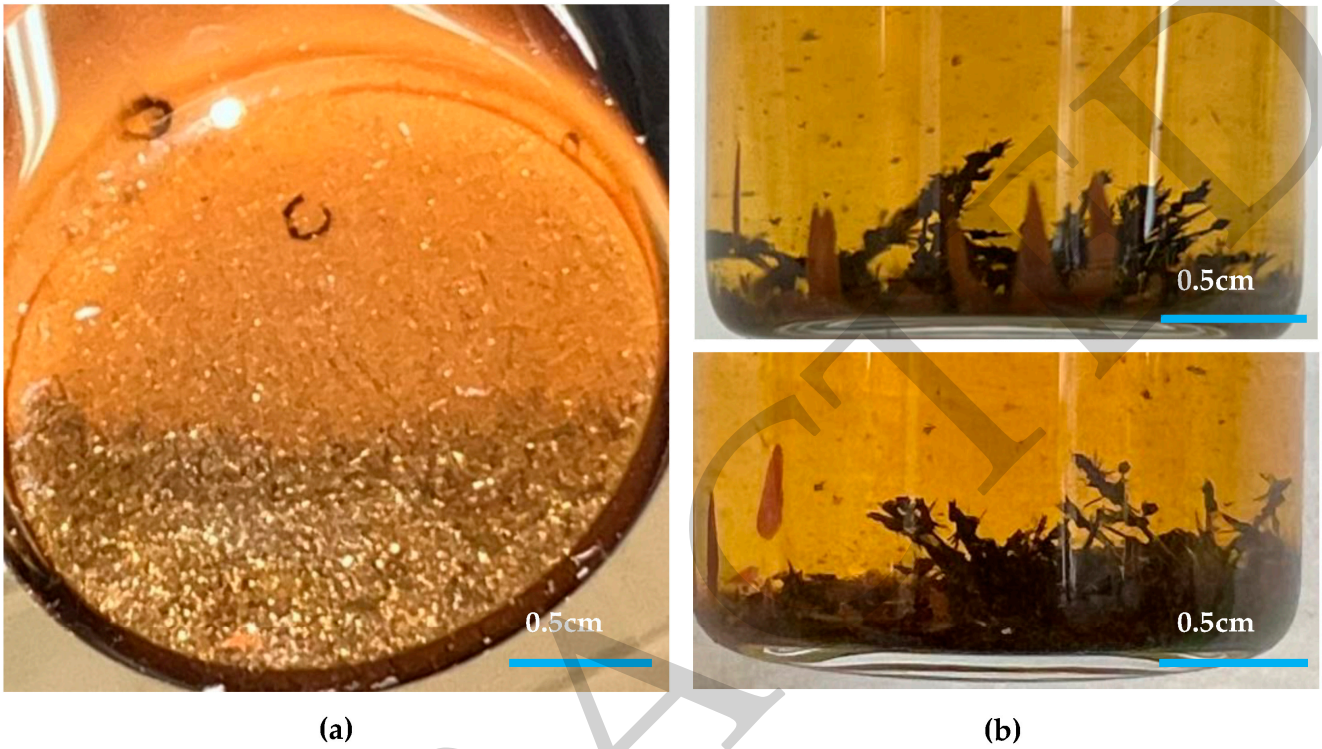

Figure 5. Effects observed with FeS: (**a**) aggregated and broken mineral particles that did not mineralize but still underwent recrystallization; (**b**) vial with both chemical gardening of FeS and malononitrile complex (with both acicular needles and nodules as a black mineral), and abiotic film growth (orange). These reference pictures were taken directly after 48 h at 90 °C. A 0.5 cm scale bar is included for reference.

Incubation at room temperature (20 °C) did show minor reactions involving the catalyst but did not include chemical gardening or mineralization. With similar morphological features forming from the FeNi and FeS catalyst additions, iron reprecipitation and catalysis may be important factors dictating the results of these incubations.

The starting FeS nanoparticles were found to be overwhelmingly in the hexagonal troilite phase via X-ray diffraction (XRD) analysis and the Jade ® software database with some minor metallic iron presence (Figure 6a). XRD was performed on the sample with the unreacted FeS from a room temperature acetonitrile reaction acting as a baseline to determine mineral identity. The troilite FeS phase is rarely produced in the Earth's crust and is most often delivered to Earth via extraterrestrial sources [28,29]. Of the metals and minerals that were altered in the reaction with organic nitriles, there was what was believed to be dissolution and reprecipitation of the iron in the reacted FeS. XRD analysis on the reacted FeS (with malononitrile and sodium formate at 90 °C) revealed a novel organic–iron complex (Figure 6b). The phase ID was unable to match perfectly with any preexisting minerals and mineral complexes in the Jade ® software database. The potential minerals that were the closest matches to the XRD spectra were consistent with Fe^{2+} to Fe^{3+}, supporting the hypothesis of hydrolysis from iron oxidation. One of the strongest candidates was parabutlerite ($Fe^{3+}SO_4(OH)\cdot H_2O$), an orthorhombic iron sulfate [51]. Parabutlerite has been shown to form with goethite under hydrothermal conditions, such as the prebiotic setup used here [52] and has been found in sulfide ores wherein the original mineral could

originate [53]. This would mean a dissolution of Fe^{2+} and S^{2-} within the aqueous solution and reprecipitation into a new oxidation state. In addition, previous work has shown that Fe^{2+}/Fe^{3+} systems may facilitate reductive organic molecule formations and be apt to chemical gardening in laboratory settings [54–56]. There may also be a mix of sulfates forming in the mineral phase, including ammonium sulfate and sodium iron sulfate. Overall, the FeS physical changes observed in this prebiotic setup was an amorphous organic–iron complex that did not have a set identity, as opposed to the troilite precursor, but is hypothesized to contain the oxidized form of iron, namely, Fe^{3+}.

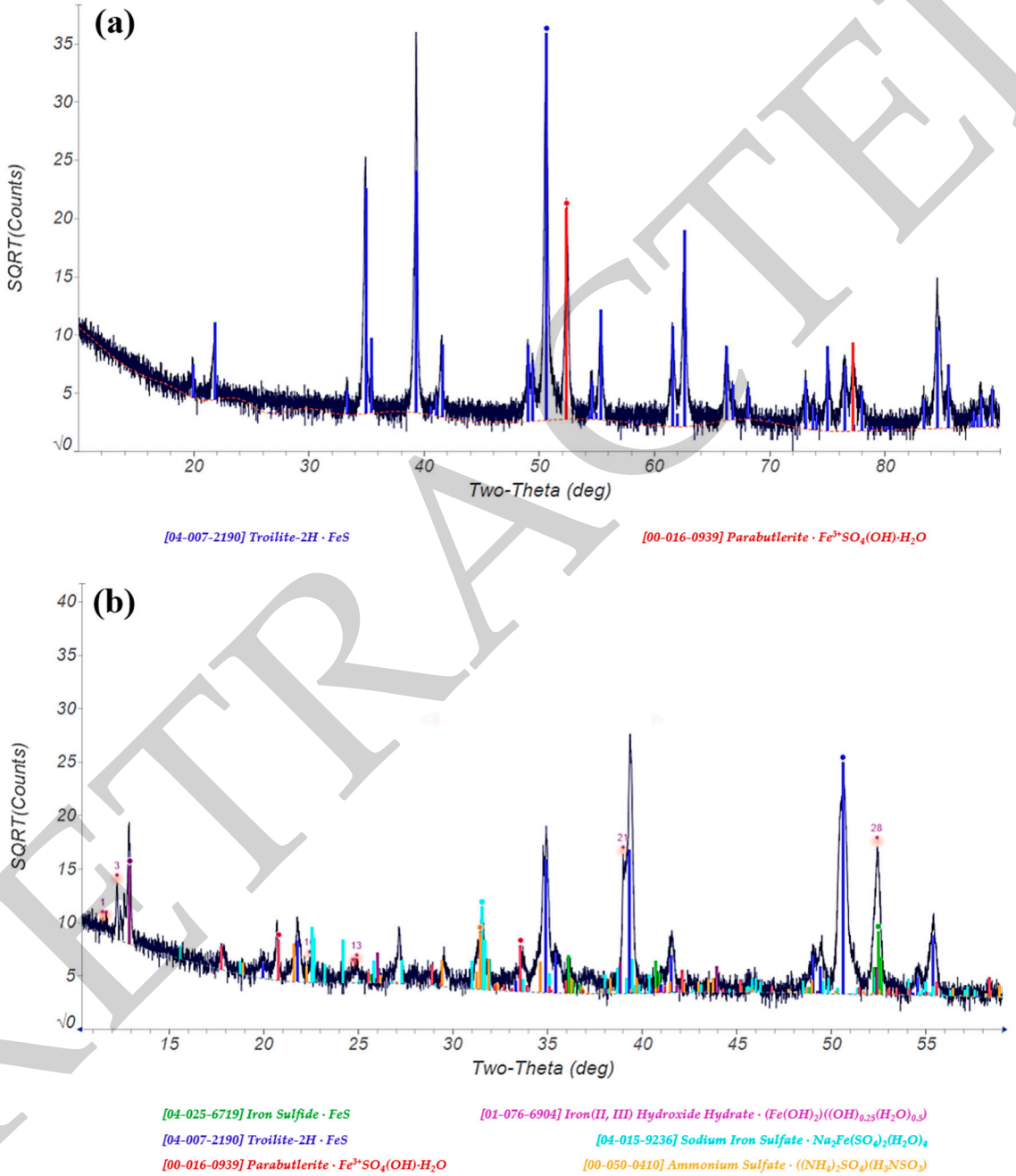

Figure 6. XRD analysis with FeS. (**a**) Unreacted FeS used with acetonitrile to be used as a control. The XRD spectrum is in black, and the red and blue lines indicate the best fit compounds from the Jade® spectra library. (**b**) Reacted FeS used with malononitrile. The XRD spectrum is in black, and the colored lines indicate the partial identity matches from the Jade® spectra library. Note that the inclusion of sodium as a compound constituent derives from the sodium formate reductant.

3.5. TiO_2 and Al_2O_3 Addition Observations

Titanium oxide (TiO_2) and aluminum oxide (Al_2O_3) both acted as a catalyst to form dark, almost viscous, insoluble products from malononitrile (Figure 7). Our results showed that TiO_2 and Al_2O_3 produced similar products with fallout of visible insoluble polymers that had a tar-like consistency. Neither TiO_2 nor Al_2O_3 catalyzed long chain dinitrile polymerization as seen with previous additions, such as metallic nickel.

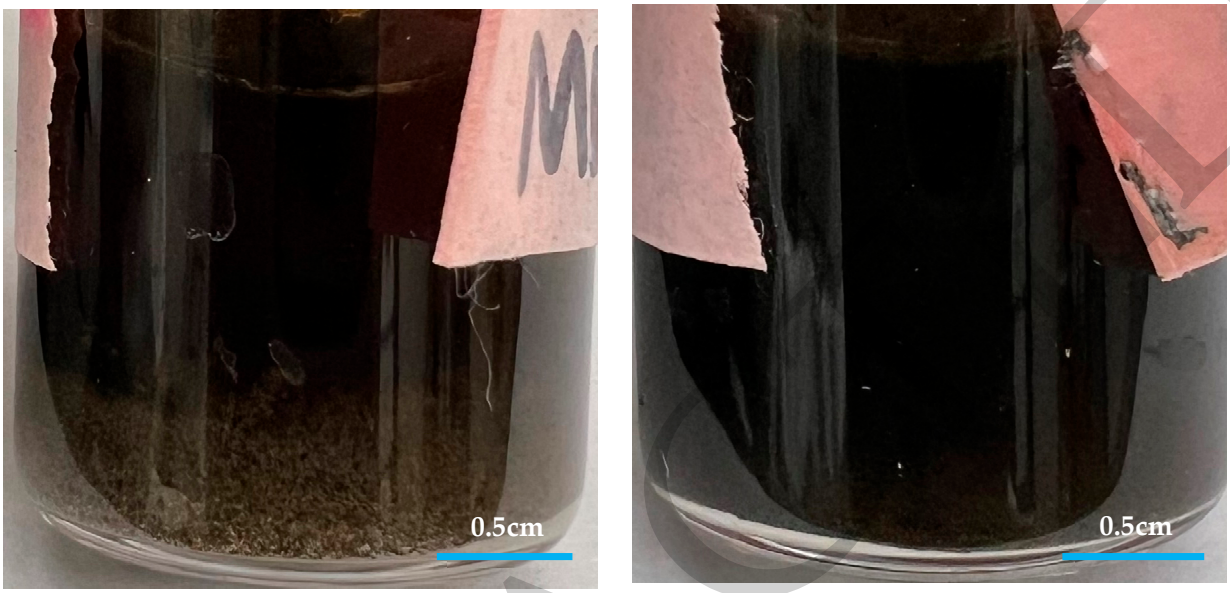

(**a**) (**b**)

Figure 7. Effects observed with oxide mineral catalysts: (**a**) TiO_2 catalytic effects; (**b**) Al_2O_3 catalytic effects. The dark material evident in both catalyst reactions is the insoluble precipitate. Reference pictures were taken directly after 48 h at 90 °C. A 0.5cm scale bar is included for reference.

3.6. Dependence on Dinitriles for Polymerization

In order to examine the dependence on a molecule with two nitrile groups for polymerization and other reactions, malononitrile ($C_3H_2N_2$) was tested in parallel to acetonitrile (CH_2CN). The dinitrile groups on malononitrile provide building blocks for long strand polymers that may link to one another and potentially outcompete other reactions. Acetonitrile is not known to polymerize with itself easily, and the terminal methyl group rarely interacts with the nitrile group on a second molecule. Thus, the limited ability of the acetonitrile nitrile group to polymerize into insoluble products makes it a strong comparison candidate in understanding malononitrile's polymerization patterns.

Under hydrothermal conditions, as stated above, malononitrile polymerized into visible particles when combined with reductants (H_2 gas and sodium formate with no metal/mineral addition) or if in the presence of an oxide, metallic nickel, and FeNi alloy. Little to no polymerization occurred with either malononitrile or acetonitrile when incubated with FeS, rhodium, or cobalt. For acetonitrile, no visible change occurred in the solution or to the metal/mineral nanoparticles under any conditions, and there was no obstruction within the solution after 48 h at high temperatures. All additions, including cobalt (Figure 8a), FeS (Figure 8b), TiO_2 (Figure 8c), and Al_2O_3 (Figure 8d), remained unaltered and did not undergo any chemical gardening. The same lack of visible change in metals and minerals was observed after incubation at room temperature.

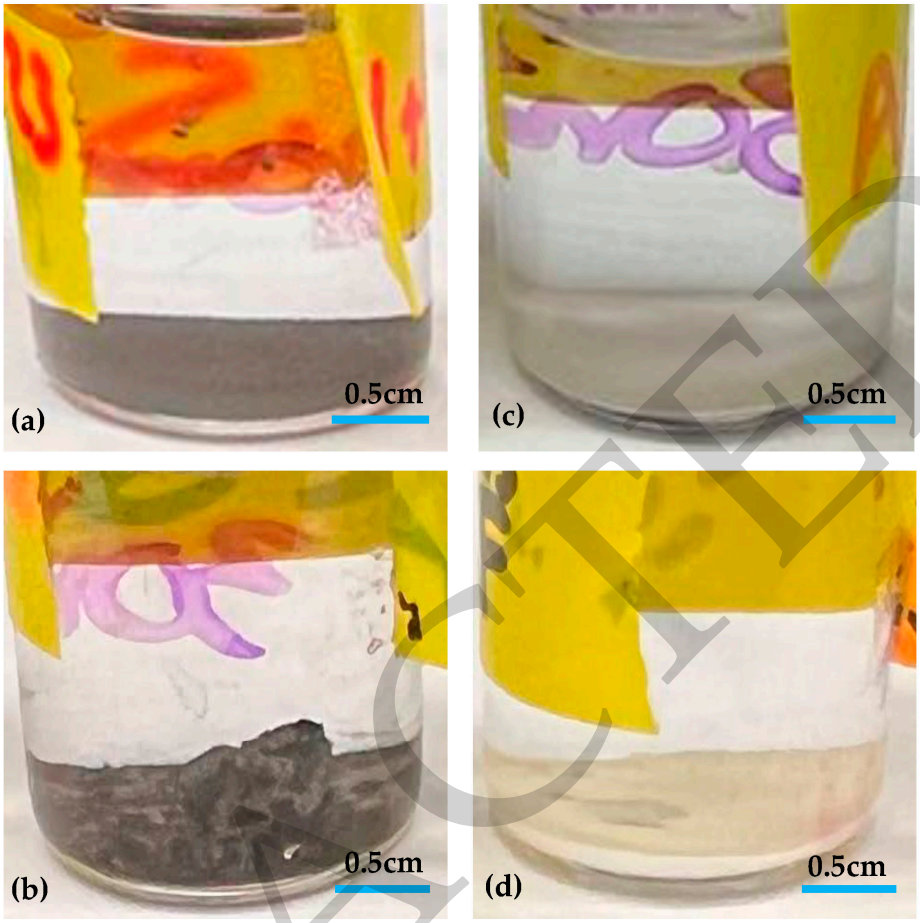

Figure 8. Representative metal nanoparticles incubated with acetonitrile: (**a**) cobalt; (**b**) FeS; (**c**) TiO_2; (**d**) Al_2O_3. Reference pictures were taken directly after 48 h at 90 °C. A 0.5 cm scale bar is included for reference.

3.7. Identification of Soluble Products

^{1}H-NMR was the primary method used to identify products reacting with the nitriles with metals and minerals under hydrothermal anoxic conditions. The ^{1}H-NMR spectra helped form a basis to compare how much product formation and insoluble polymerization occurred under each temperature and metal or mineral addition. While there was some alternative product formation, the oxide minerals were more apt to form insoluble, tar-like products from malononitrile. Neither the insoluble polymers nor the tar-like products were able to be measured by ^{1}H-NMR, and their chemical structures could not be discerned. The identification of the structures of insoluble products was beyond the scope of this study and requires future investigation.

Soluble products measured via ^{1}H-NMR primarily landing within a 3 ppm region of chemical shifts (between 1 ppm and 4 ppm) point towards reduction and polymerization into insoluble products of the nitrile group. In the results, this region was indicative of products with new functional groups formed during reduction, hydrolysis, and/or polymerization involving the nitrile group. Notable possibilities for functional groups and their common ppm ranges are listed below (Table 3). The addition of oxygen as an aldehyde functional group was unlikely, as the proton always falls above 9 ppm, which was not seen in any measured spectra (Figures 9 and S1–S3). Note that the ^{1}H-NMR analysis of malononitrile catalysis with first row transition metals—including iron-bearing nanoparticles, cobalt, and nickel-bearing nanoparticles—was hindered by their magnetic properties. The nanoparticle size and polymer formation that trapped the nanoparticles made complete removal of the reagent not possible, even with centrifugation. These metal-

including spectra have some broader peaks, or the sodium formate peak is distinctly shifted upfield and broadened (Figures S3 and S5).

Table 3. Common ^{1}H-NMR shifts (ppm) with D_2O solvent.

Functional Group (Hydrogen)	Structure	δ (ppm) *
Alcohol	R-O**H** R-C**H**$_2$-OH	0.5–5.0 3.3–4.0
Aldehyde	R-C(=O)-**H**	9.5–9.9
Alkane	R-C**H**$_3$ R-C**H**$_2$-R R$_3$-C-**H**	0.8–1.0 1.2–1.4 1.4–1.7
Amide	R-C(=O)-N**H**$_2$ C**H**-C(=O)-NH$_2$	5.9–6.3 2.0–2.2
Amine	R-N**H**$_2$	0.5–5.0
Aromatic (nitrogen heterocycle)	Ar=C**H**-CR$_2$ Ar-N**H** CR$_2$-C**H**$_2$-NR	6.0–8.0 6.0–9.5 1.6–3.3
Carbonyl	R-C(=O)-C**H**$_3$	2.1–2.6
Carboxylic Acid	R-C(=O)-O**H** R**H**-C(=O)-OH	Cannot see due to proton exchange 2.5–3.0
Nitrile	**H**-C-C≡N	2.0–3.0

* modified from [57,58].

Major products were defined as having an intensity of ≥25,000 although chemical shift values for all notable peaks are given regardless of intensity (Figures S2–S5). Any multiplet more than a doublet (triplet, quartet, etc.) above this threshold was marked with an asterisk. A chemical shift in a distinct multiplet could denote reduction from the nitrile and formation of a reduced functional group (either through catalytic reduction or during polymerization). Note that there is an effect of the pH and metal presence on chemical shifts. The sodium formate peak at 8.35 ppm was not included in the count of peaks, as it was in excess and not a nitrile product.

Malononitrile itself primarily undergoes hydrolysis into malonamide and malonate (Figure 9a). The ^{1}H-NMR spectra contained 14 major singlet peaks, 1 doublet peak, and 1 triplet peak. The majority of major peaks was located in the 1–4 ppm range, including the peaks for malonamide, malonate, and unreacted malononitrile. Dinitrile reaction with rhodium generated a range of new products alongside malonamide and malonate (Figure 9b). The ^{1}H-NMR spectra contained 26 major singlet peaks, 1 doublet, and 3 multiplets. Unlike malononitrile hydrolysis and degradation alone, the rhodium had a wider range of peaks that spanned up to 7 ppm at high intensities. The addition of FeS to reactions showed 17 major singlet peaks and 1 doublet peak. The reaction products showed similar trends to the rhodium reactions; however, the lack of ^{1}H-NMR detection may be due in part to the magnetic properties of FeS contaminating analysis samples in a similar fashion to the broadening of peaks (Figure 9c). Dinitrile catalysis with a metal oxide such as Al_2O_3 (Figure 9d) presented similarly to the rhodium and other non-oxide, catalytic-style reactions; however, the intensity was far lower and was not counted as major products formed. The ^{1}H-NMR spectra of Al_2O_3 contained six major singlet peaks, one doublet, one doublet of a doublet, and two multiplets. None of the chemical shifts for any of the reactions fell above sodium formate's 8.35 ppm peak, indicating the lack of deshielded, electron-poor compounds. Due to the relative concentrations of hydrolysis products and unreacted malononitrile, this may be indicative that Al_2O_3 and TiO_2 are poor catalyst choices when looking for minerals and metals to catalyze and promote prebiotic reactions; on the other hand, the group nine transition metals may prove optimal as they do not have

insoluble precipitate or polymer formation and efficiently provide numerous reactions alternative to hydrolysis.

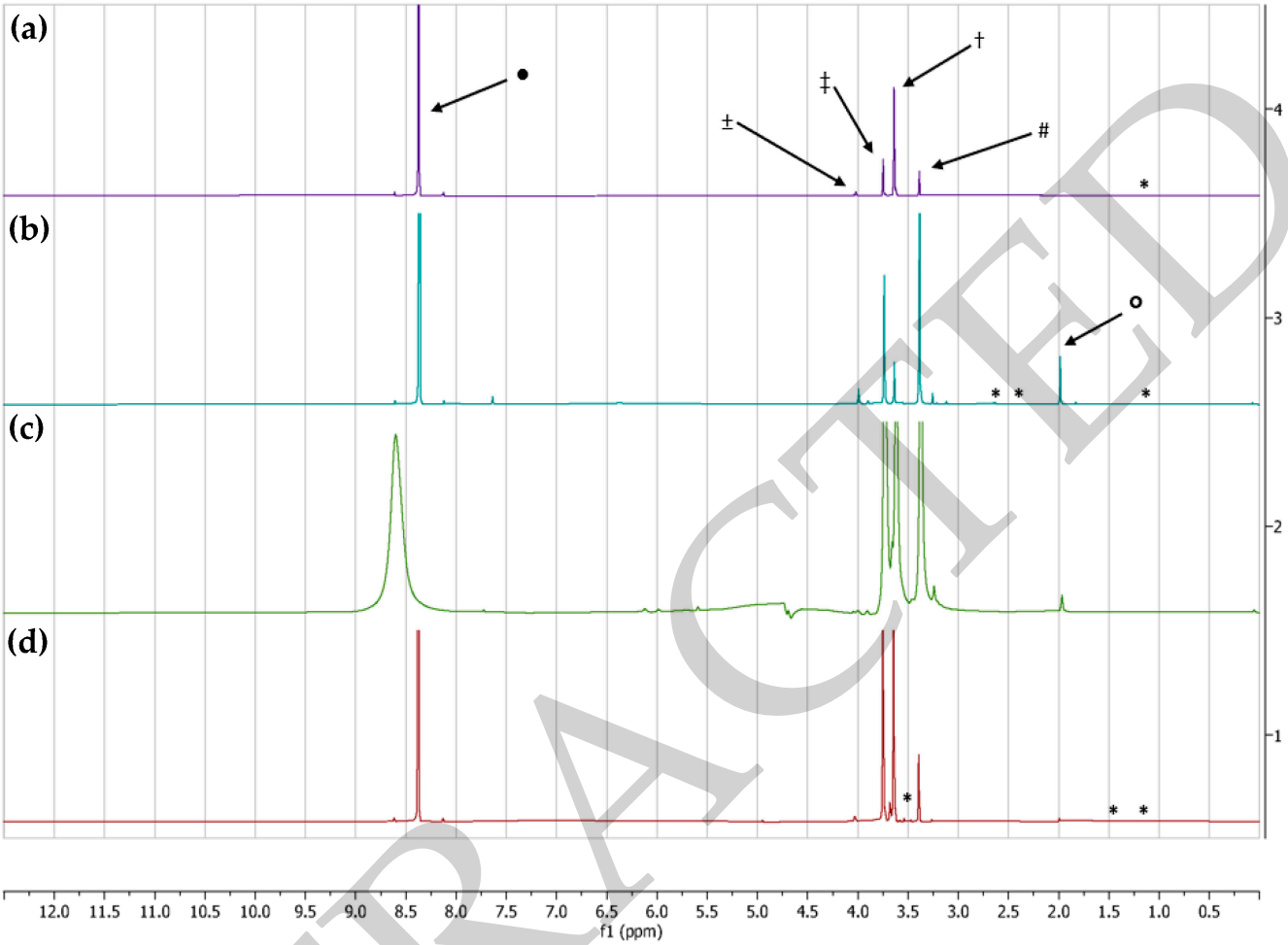

Figure 9. Selected ^{1}H-NMR spectra of malononitrile after 48 h at 90 °C: (**a**) malononitrile and sodium formate; (**b**) malononitrile, sodium formate, and rhodium; (**c**) malononitrile, sodium formate, and FeS; (**d**) malononitrile, sodium formate, and Al_2O_3. Major suspected hydrolysis product peaks are: ± = malononitrile, † = malonamide, # = malonate (malonic acid), ‡ = malonic acid monoamide, and ○ = amide functional group. ● = sodium formate. * = multiplet locations. Expanded spectra with detailed chemical shifts and multiplet locations can be found in Figures S2–S5.

While all additions of metals or minerals followed similar peaks of non-hydrolysis products with reaction with malononitrile, group nine transition metals displayed the most variety while also having the least amount of polymerization to insoluble products that could not be measured. The reactions showed spectra shifts higher than 6 ppm, while malononitrile alone did not, which may indicate the cyclization of malononitrile into a nitrogen heterocyclic structure. This is further supported by the lack of spectra upfield from ~4.5 ppm in the acetonitrile reactions, showing that multiple carbons are needed for cyclization (Figures S2 and S4).

Acetonitrile incubation at 90 °C for 48 h did not produce any polymerization to insoluble products based on visual observations. This is to be expected as only one side of the acetonitrile molecule will have a nitrile group to participate in reactions, and the C–H bonds are most likely left unreacted. In the samples studied here, acetonitrile was resistant to most additions and either remained unreacted or only underwent a small amount of hydrolysis to acetic acid and acetamide, as shown by the ^{1}H-NMR of soluble products (Figures S2 and S4). In the case of FeS and nickel at 90 °C, some products beyond hydrolyzed

molecules could be found, including ethanol at 1.2 ppm and 3.5 ppm, and potentially ethylamine at 2.9 ppm, as supported by the presence of a multiplet (Figures S2 and S4). The reaction of FeS and nickel with acetonitrile at 90 °C to form ethanol and ethylamine indicates that reduction of the nitrile group is possible under prebiotic conditions, and that malononitrile may also be undergoing reduction, but identification requires further studies.

3.8. Geologic Implications and Significance

While metallic iron and iron–nickel ores are known in serpentinites, nanopowder metals and minerals in a pure form are uncommon in crustal systems. This study used nanoparticle metals and minerals as a means to investigate whether it is possible to have a nitrile reaction other than polymerization or hydrolysis. By using nanoparticles, the surface area of the metals and minerals was increased, and thus reaction rates were increased. In an early Earth hydrothermal system, it is reasonable to imagine the organic material flowing over a mineral or metal-bearing basaltic rock for thousands of years. The reaction rate would likely be on a slower timescale than is feasible in a laboratory setting. In a hydrothermal environment of early Earth, reactions would be occurring in a flow-through manner, which might be different than the batch reactions we studied here. However, because the timescale of circulation flow through the oceanic crust is on the order of thousands of years with constant contact with rock surfaces, the chemical observations found here are likely to be relevant.

4. Conclusions

Metals and minerals in mafic to ultramafic basaltic systems have proven to be effective in driving a wide range of prebiotic nitrile reactions. In early Earth oceans, these metals and minerals would have provided alternative reaction outcomes beyond self-polymerization and hydrolysis, including potential cyclization and reduction of the nitrile groups. Here, we identified common observational trends amongst elemental metals, metal oxides, and geologically relevant minerals that could have facilitated prebiotic reactions via catalysis and reprecipitation/mineralization of the metal complexing with an organic. However, even given the accessibility of such reagents, hydrolysis into amides and carboxylic acids would have still dominated the end products of reactive nitrile compounds. While this result may hinder the amount of alternative products, future studies may reveal compounds not fully utilized before due to their perceived lack of formation. For example, the nitrile groups of aminomalononitrile may both reduce into alcohols to form the molecule serinol.

The observed nucleation of organic products onto the group nine metal nanoparticles may serve as a viable concentration method for prebiotic molecules in hydrothermal systems and would be an interesting point of study. As the concentrations of HCN and HCN polymers would be relatively lower in the early Earth ocean at a rain-out rate of 1×10^7 cm^{-2} s^{-1} [15] than what we used during laboratory experiments here, a mechanism for increasing local concentrations would be valuable for further reactions of products. If the products do complex with metals in hydrothermal basaltic rocks, this may prove to be a valuable way to localize molecules and increase the likelihood of interaction and reaction.

Looking to further applications and future research, the wide range of physical outcomes may lead to a revisit of what metal catalysts or reagents are best in a prebiotic system. Iron (II) sulfide (FeS) is the most geologically relevant metal/mineral in this study and supports a plausible scenario of mineralization into parabutlerite and sulfate minerals. This also presents the potential for reduction coupled with the building of mineralogical chemical gardens. Nickel and iron metals or minerals are known to have been prevalent in early Earth oceans and are easily obtained commercially, making for an attractive choice of reagent. The group nine transition metal nanoparticles display unique morphologies where organics complex and nucleate to their surface. Both TiO_2 and Al_2O_3 catalyzed formation of insoluble products and tar-like polymers. The observed chemical gardening was an unexpected phenomenon that occurred with the FeS, FeNi, and rhodium additions. Most chemical gardening occurs due to a redox gradient of solution with iron and iron

minerals [54,55]. In laboratory settings, chemical gardens are also grown using metal-ion salts injected into an anionic solution, most often with silicates [50]. FeNi and elemental rhodium are uncharged and were not expected to act as cations; FeS utilizes Fe^{2+}. The apparent complexing with organic material in the solution indicates that the metals are participating as reagents in the reaction and may be a pathway to new meta-complexed organics that have not been noted to have prebiotic relevance before to our knowledge.

Overall, there is a need for prebiotically plausible metals and minerals with their associated organic compound products to be compiled [59]. Each addition of metal or mineral was able to produce a wide range of small organic products with ^{1}H-NMR spectra peaks following the trends of upfield and shielded molecules, and identification of exact product differences may warrant more exploration. Future research may expand past categorizing the general reduction or polymerization caused by the metals themselves and into the prebiotic organic synthesis of various compounds. This includes investigating the HCN trimer aminomalononitrile as a more prebiotically relevant molecule and what products it may produce when in contact with metals or minerals.

Supplementary Materials: The following supporting information can be downloaded at: https://www.mdpi.com/article/10.3390/life13071524/s1, Figure S1: ^{1}H-NMR Analysis of Standards; Figure S2: ^{1}H-NMR Analysis of Acetonitrile Reactions at 90 °C; Figure S3: ^{1}H-NMR Analysis of Malononitrile Reactions at 90 °C; Figure S4: ^{1}H-NMR Analysis of Acetonitrile Reactions at 20 °C; Figure S5: ^{1}H-NMR Analysis of Malononitrile Reactions at 20 °C; Table S1: XRD Angles of FeS Analysis.

Author Contributions: Conceptualization, M.S. and C.H.; methodology, M.S. and C.H.; investigation, M.S.; resources, C.H.; data curation, M.S.; writing—original draft preparation, M.S.; writing—review and editing, M.S. and C.H.; supervision, C.H.; project administration, C.H.; funding acquisition, C.H. All authors have read and agreed to the published version of the manuscript.

Funding: This research was funded by NASA Astrobiology NfoLD (Network for Life Detection), grant number 80NSSC18K1140 and by the NSF, grant number EF-1724099.

Institutional Review Board Statement: Not applicable.

Informed Consent Statement: Not applicable.

Data Availability Statement: Not applicable.

Acknowledgments: We would like to acknowledge Laurie Barge (NASA Jet Propulsion Laboratory), for her insight into hydrothermal chemical gardening, and Peter Heaney (Pennsylvania State University), for advice on mineral growth. We also would like to acknowledge Nicole Wonderling (Pennsylvania State University), for her XRD technical expertise, and E. Barlow and G. Soares, for comments during the editing stage. Finally, we would like to thank our three anonymous reviewers and their insightful comments and revision suggestions.

Conflicts of Interest: The authors declare no conflict of interest.

References

1. Shock, E.L. Hydrothermal Systems as Environments for the Emergence of Life. In *Novartis Foundation Symposium*; Wiley: Hoboken, NJ, USA, 1996; pp. 40–60.
2. Janecky, D.R.; Seyfried, W.E. Hydrothermal serpentinization of peridotite within the oceanic crust: Experimental investigations of mineralogy and major element chemistry. *Geochim. Cosmochim. Acta* **1986**, *50*, 1357–1378. [CrossRef]
3. Kobayashi, K.; Yanagawa, H. Submarine Hydrothermal Vents as Possible Sites of the Origin of Life. In *Biological Systems Under Extreme Conditions: Structure and Function*; Springer: Berlin/Heidelberg, Germany, 2002; pp. 221–238.
4. Kelley, D.S.; Karson, J.A.; Blackman, D.K.; Früh-Green, G.L.; Butterfield, D.A.; Lilley, M.D.; Olson, E.N.; Schrenk, M.O.; Roe, K.J.; Lebon, G.T.; et al. An off-axis hydrothermal vent field near the Mid-Atlantic Ridge at 30° N. *Nature* **2001**, *412*, 145–149. [CrossRef] [PubMed]
5. Shock, E.L.; Schulte, M.D. Organic synthesis during fluid mixing in hydrothermal systems. *J. Geophys. Res.* **1998**, *103*, 28513–28527. [CrossRef]
6. Rimmer, P.B.; Shorttle, O. Origin of Life's Building Blocks in Carbon- and Nitrogen-Rich Surface Hydrothermal Vents. *Life* **2019**, *9*, 12. [CrossRef]
7. Islam, S.; Bučar, D.; Powner, M.W. Prebiotic selection and assembly of proteinogenic amino acids and natural nucleotides from complex mixtures. *Nat. Chem.* **2017**, *9*, 584–589. [CrossRef]

8. Ruiz-Bermejo, M.; De La Fuente, J.; Pérez-Fernández, C.; Mateo-Martí, E. A Comprehensive Review of HCN-Derived Polymers. *Processes* **2021**, *9*, 597. [CrossRef]
9. Villafañe-Barajas, S.A.; Ruiz-Bermejo, M.; Rayo-Pizarroso, P.; Colín-García, M. Characterization of HCN-Derived Thermal Polymer: Implications for Chemical Evolution. *Processes* **2020**, *8*, 968. [CrossRef]
10. Holm, N.G.; Neubeck, A. Reduction of nitrogen compounds in oceanic basement and its implications for HCN formation and abiotic organic synthesis. *Geochem. Trans.* **2009**, *10*, 9. [CrossRef]
11. Li, Y.; Kitadai, N.; Nakamura, R. Chemical Diversity of Metal Sulfide Minerals and Its Implications for the Origin of Life. *Life* **2018**, *8*, 46. [CrossRef]
12. Bougault, H. Distribution of First Series Transition Metals in Rocks Recovered during DSDP Leg 22 in the Northeastern Indian Ocean. *Initial Rep. Deep Sea Drill. Proj.* **1974**, *22*, 449–457.
13. Wade, J.; Wood, B. Core formation and the oxidation state of the Earth. *Earth Planet. Sci. Lett.* **2005**, *236*, 78–95. [CrossRef]
14. Ranjan, S.; Todd, Z.R.; Rimmer, P.B.; Sasselov, D.; Babbin, A.R. Nitrogen Oxide Concentrations in Natural Waters on Early Earth. *Geochem. Geophys. Geosystems* **2019**, *20*, 2021–2039. [CrossRef]
15. Tian, F.; Kasting, J.F.; Zahnle, K. Revisiting HCN formation in Earth's early atmosphere. *Earth Planet. Sci. Lett.* **2011**, *308*, 417–423. [CrossRef]
16. Miller, S.L. Production of Some Organic Compounds under Possible Primitive Earth Conditions1. *J. Am. Chem. Soc.* **1955**, *77*, 2351–2361. [CrossRef]
17. Borquez, E.; Cleaves, H.J.; Lazcano, A.; Miller, S.L. An Investigation of Prebiotic Purine Synthesis from the Hydrolysis of HCN Polymers. *Orig. Life Evol. Biosph.* **2005**, *35*, 79–90. [CrossRef]
18. Thissen, H.; Evans, R.; Ball, V. Films and Materials Derived from Aminomalononitrile. *Processes* **2021**, *9*, 82. [CrossRef]
19. Rouxel, O.; Bekker, A.; Edwards, K.J. Iron Isotope Constraints on the Archean and Paleoproterozoic Ocean Redox State. *Science* **2005**, *307*, 1088–1091. [CrossRef]
20. Frey, P.A.; Reed, G.W. The Ubiquity of Iron. *ACS Chem. Biol.* **2012**, *7*, 1477–1481. [CrossRef]
21. Pechersky, D.M.; Markov, G.P.; Tselmovich, V.A. Pure iron and other magnetic minerals in meteorites. *Sol. Syst. Res.* **2015**, *49*, 61–71. [CrossRef]
22. Liao, L.; Xu, X.; Jiang, X.; Wang, C.; Zhang, D.; Ni, J.; Wu, M. Microbial diversity in deep-sea sediment from the cobalt-rich crust deposit region in the Pacific Ocean. *FEMS Microbiol. Ecol.* **2011**, *78*, 565–585. [CrossRef]
23. Greenough, J.D.; Fryer, B.J. Distribution of Gold, Palladium, Platinum, Rhodium, Ruthenium, and Iridium in Leg 115 Hotspot Basalts: Implications for Magmatic Processes. *Proc. Ocean Drill. Program* **1990**, *115*, 71–84.
24. Ryzhenko, B.N.; Kovalenko, N.I.; Prisyagina, N.I. Titanium complexation in hydrothermal systems. *Geochem. Int.* **2006**, *44*, 879–895. [CrossRef]
25. Li, P.R.; Perreau, K.A.; Covington, E.; Song, C.; Carmichael, G.R.; Grassian, V.H. Heterogeneous reactions of volatile organic compounds on oxide particles of the most abundant crustal elements: Surface reactions of acetaldehyde, acetone, and propionaldehyde on SiO_2, Al_2O_3, Fe_2O_3, TiO_2, and CaO. *J. Geophys. Res.* **2001**, *106*, 5517–5529. [CrossRef]
26. Brey, W.S.; Krieger, K.A. The Surface Area and Catalytic Activity of Aluminum Oxide. *J. Am. Chem. Soc.* **1949**, *71*, 3637–3641. [CrossRef]
27. Pour, A.N.; Housaindokht, M.R. Effects of metallic cobalt crystal phase on catalytic activity of cobalt catalysts supported on carbon nanotubes in Fischer–Tropsch synthesis. *Prog. React. Kinet. Mech.* **2019**, *44*, 316–323. [CrossRef]
28. Carpenter, R.J.; Desborough, G.A. Range in solid solution and structure of naturally occurring troilite and pyrrhotite. *Am. Mineral.* **1964**, *49*, 1350–1365.
29. Kaplan, I.R.; Hulston, J. The isotopic abundance and content of sulfur in meteorites. *Geochim. Cosmochim. Acta* **1966**, *30*, 479–496. [CrossRef]
30. Heift, D. Iron Sulfide Materials: Catalysts for Electrochemical Hydrogen Evolution. *Inorganics* **2019**, *7*, 75. [CrossRef]
31. Rickard, D.; Luther, G.W. Chemistry of Iron Sulfides. *Chem. Rev.* **2007**, *107*, 514–562. [CrossRef]
32. Yang, Y.; Chen, T.; Sumona, M.; Gupta, B.; Sun, Y.; Zhan, X.; Zhan, X. Utilization of iron sulfides for wastewater treatment: A critical review. *Rev. Environ. Sci. Bio Technol.* **2017**, *16*, 289–308. [CrossRef]
33. Wang, W.; Yang, B.; Qu, Y.; Liu, X.; Su, W. FeS/S/FeS2Redox System and Its Oxidoreductase-like Chemistry in the Iron-Sulfur World. *Astrobiology* **2011**, *11*, 471–476. [CrossRef]
34. Lai, S.; Lin, H.; Lin, Y.; Yu, T. Hydrolysis of ammonia–borane catalyzed by an iron–nickel alloy on an SBA-15 support. *Int. J. Hydrog. Energy* **2013**, *38*, 4636–4647. [CrossRef]
35. Taylor, D.; Smith, P.; Dowden, D.A.; Kemball, C.; Whan, D.A. Ammonia synthesis and related reactions over iron-cobalt and iron-nickel alloy catalysts. Part I. Catalysts reduced at 853 K. *Appl. Catal.* **1982**, *3*, 161–176. [CrossRef]
36. Kukushkin, V.Y.; Pombeiro, A.J.L. Metal-mediated and metal-catalyzed hydrolysis of nitriles. *Inorganica Chim. Acta* **2005**, *358*, 1–21. [CrossRef]
37. Staskun, B.; Van Es, T. The reduction of nitriles to aldehydes: Applications of Raney nickel/sodium hypophosphite monohydrate, of Raney nickel/formic acid, or of Raney(Ni/Al) alloy/formic acid, respectively. *S. Afr. J. Chem.* **2008**, *61*, 144–156. [CrossRef]
38. Bodnar, Z.; Mallat, T.; Petró, J. Reductive hydrolysis of nitriles to aldehydes by precipitated nickel on iron or aluminium. *J. Mol. Catal.* **1991**, *70*, 53–64. [CrossRef]

39. Adkins, H.; Billica, H.R. The Preparation of Raney Nickel Catalysts and their Use Under Conditions Comparable with Those for Platinum and Palladium Catalysts. *J. Am. Chem. Soc.* **1948**, *70*, 695–698. [CrossRef]
40. Cook, P.F. The Reduction of Aldehydes and Ketones with Nickel—Aluminum Alloy in Aqueous Alkaline Solution. *J. Org. Chem.* **1962**, *27*, 3873–3875. [CrossRef]
41. Bonnier, J.M.; Damon, J.; Masson, J. Raney nickel as a selective catalyst for aldehyde reduction in the presence of ketones. *Appl. Catal.* **1987**, *30*, 181–184. [CrossRef]
42. Barrero, A.F.; Alvarez-Manzaneda, E.; Chahboun, R.; Meneses, R. Chemoselective Reduction of Aldehydes in the Presence of Ketones Utilizing Raney Nickel. *Synlett* **2000**, *2000*, 197–200. [CrossRef]
43. Kidwai, M.; Bansal, V.; Saxena, A.; Shankar, R.; Mozumdar, S. Ni-nanoparticles: An efficient green catalyst for chemoselective reduction of aldehydes. *Tetrahedron Lett.* **2006**, *47*, 4161–4165. [CrossRef]
44. Beyer, H.; Emmerich, J.; Chatziapostolou, K.; Köhler, K. Decomposition of nitrous oxide by rhodium catalysts: Effect of rhodium particle size and metal oxide support. *Appl. Catal. A Gen.* **2011**, *391*, 411–416. [CrossRef]
45. Gu, Y.; Norton, J.R.; Salahi, F.; Lisnyak, V.G.; Zhou, Z.; Snyder, S.A. Highly Selective Hydrogenation of C=C Bonds Catalyzed by a Rhodium Hydride. *J. Am. Chem. Soc.* **2021**, *143*, 9657–9663. [CrossRef] [PubMed]
46. Barge, L.M.; Cardoso SS, S.; Cartwright JH, E.; Cooper, G.M.; Cronin, L.; De Wit, A.; Doloboff, I.J.; Escribano, B.; Goldstein, R.E.; Haudin, F.; et al. From Chemical Gardens to Chemobrionics. *Chem. Rev.* **2015**, *115*, 8652–8703. [CrossRef]
47. Batista, B.C.; Steinbock, O. Chemical gardens without silica: The formation of pure metal hydroxide tubes. *Chem. Commun.* **2015**, *51*, 12962–12965. [CrossRef]
48. Pampalakis, G. The Generation of an Organic Inverted Chemical Garden. *Chem. Eur. J.* **2016**, *22*, 6779–6782. [CrossRef]
49. Barge, L.M.; Jones, J.R.; Pagano, J.J.; Martínez, E.; Bescup, J. Three-Dimensional Analysis of a Simulated Prebiotic Hydrothermal Chimney. *ACS Earth Space Chem.* **2020**, *4*, 1663–1669. [CrossRef]
50. Cartwright JH, E.; Escribano, B.; Sainz-Díaz, C.I. Chemical-Garden Formation, Morphology, and Composition. I. Effect of the Nature of the Cations. *Langmuir* **2011**, *27*, 3286–3293. [CrossRef]
51. Fanfani, L.; Nunzi, A.; Zanazzi, P.F. The Crystal Structure of Butlerite. *Am. Mineral.* **1971**, *56*, 751–757.
52. Fang, F.; Jia, Y.; Wu, P.J.; Zhang, Q.; Jiang, Y.; Zhou, S.; Peng, D. Facile one-pot preparation of goethite/parabutlerite nanocomposites and their removal properties and mechanism toward As(V) ions. *Appl. Surf. Sci.* **2015**, *324*, 355–362. [CrossRef]
53. Gablina, I.F.; Dobretzova, I.G.; Laiba, A.A.; Narkevsky, E.V.; Maksimov, F.; Kuznetsov, V.V. Specific Features of Sulfide Ores in the Pobeda Hydrothermal Cluster, Mid-Atlantic Rise 17°07′–17°08′ N. *Lithol. Miner. Resour.* **2018**, *53*, 431–454. [CrossRef]
54. Barge, L.M.; Cardoso SS, S.; Cartwright JH, E.; Doloboff, I.J.; Flores, E.; Macías-Sánchez, E.; Sainz-Díaz, C.I.; Sobron, P. Self-assembling iron oxyhydroxide/oxide tubular structures: Laboratory-grown and field examples from Rio Tinto. *Proc. R. Soc. A Math. Phys. Eng. Sci.* **2016**, *472*, 20160466. [CrossRef] [PubMed]
55. Barge, L.M.; Flores, E.; Baum, M.M.; VanderVelde, D.G.; Russell, M.J. Redox and pH gradients drive amino acid synthesis in iron oxyhydroxide mineral systems. *Proc. Natl. Acad. Sci. USA* **2019**, *116*, 4828–4833. [CrossRef] [PubMed]
56. Barge, L.M.; Flores, E.F.; Vandervelde, D.; Weber, J.; Baum, M.J.; Castonguay, A. Effects of Geochemical and Environmental Parameters on Abiotic Organic Chemistry Driven by Iron Hydroxide Minerals. *J. Geophys. Res. Planets* **2020**, *125*, e2020JE006423. [CrossRef]
57. Hassner, A.; Michelson, M.J. NMR Spectra and Stereoisomerism in Pyrazolines. *J. Org. Chem.* **1962**, *27*, 3974–3976. [CrossRef]
58. Pavia, D.L.; Lampman, G.M.; Kriz, G.S.; Vyvyan, J.A. *Introduction to Spectroscopy*; Cengage Learning: Boston, MA, USA, 2014.
59. Prakash, M.; Weber, J.A.; Rodriguez, L.P.; Sheppard, R.Y.; Barge, L.M. Database on mineral mediated carbon reduction: Implications for future research. *Int. J. Astrobiol.* **2022**, *21*, 423–440. [CrossRef]